Recrystallization and Reactivation of Dopant Atoms in Ion-Implanted Silicon Nanowires

Naoki Fukata,[†,*] Ryo Takiguchi,[‡] Shinya Ishida,[‡] Shigeki Yokono,[‡] Shunichi Hishita,[†] and Kouichi Murakami[‡]

[†]International Center for Materials Nanoarchitectonics, National Institute for Materials Science, 1-1 Namiki, Tsukuba, 305-0044, Japan and [‡]Institute of Applied Physics, University of Tsukuba, 1-1-1 Tennodai, Tsukuba, 305-8573, Japan

ABSTRACT

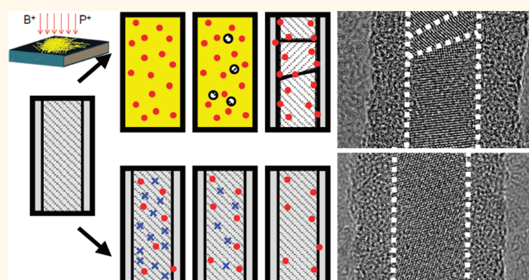

Recrystallization of silicon nanowires (SiNWs) after ion implantation strongly depends on the ion doses and species. Full amorphization by high-dose implantation induces polycrystal structures in SiNWs even after high-temperature annealing, with this tendency more pronounced for heavy ions. Hot-implantation techniques dramatically suppress polycrystallization in SiNWs, resulting in reversion to the original single-crystal structures and consequently high reactivation rate of dopant atoms. In this study, the chemical bonding states and electrical activities of implanted boron and phosphorus atoms were evaluated by Raman scattering and electron spin resonance, demonstrating the formation of p- and n-type SiNWs.

KEYWORDS: silicon nanowires · boron · phosphorus · implantation

Nanoscale silicon devices using silicon nanowires (SiNWs) such as metal-oxide semiconductor field-effect transistors (MOSFETs) require properties that allow their electrical conductivity to be controlled. Considerable efforts have been directed at developing nanoscale silicon devices such as these; however, advances in growth and impurity doping techniques are required.[1−12] Impurity doping of SiNWs or germanium nanowires (GeNWs) is generally performed *in situ* during vapor−liquid−solid (VLS) growth, which has the advantage of not inducing defects.[1−11] However, there are also certain disadvantages, such as surface doping and tapering structures created by sidewall growth, resulting in non-uniform doping along the growth direction of NWs.[9−11]

On the other hand, ion implantation is now commonly used in semiconductor manufacturing. This technique allows the precise control of dopant concentration and provides uniformity in the growth direction. In bulk Si, the introduction of dopant impurities and defects, their interaction, the recrystallization process with defect annihilation in implanted regions, and the subsequent reactivation process of dopant impurities have been extensively investigated. The recrystallization process with defect annihilation is a key point for controlling the reactivation and distribution of dopant atoms. Recently, ion implantation has also been performed in SiNWs to fabricate p- and n-type SiNW FETs.[13−18]

We have established characterization methods in recent studies to clarify the states of dopant atoms in SiNWs, specifically their bonding states and electrical activity, using micro-Raman scattering and electron spin resonance (ESR).[19−22] The results of our micro-Raman scattering measurements clearly showed boron local vibrational peaks at 618 and 640 cm^{-1} and Fano broadening of the Si optical phonon peak in SiNWs due to the high concentrations of holes that result from intensive B doping.[19,22] Raman measurements are also useful for investigating the crystallinity of SiNWs. ESR measurements at 4.2 K showed the ESR signal for conduction electrons in phosphorus-doped SiNWs.[20,22] These results clearly proved that B and P atoms had been doped in the crystalline Si core of SiNWs and were electrically activated at these sites. ESR is also a sensitive method for detecting defects caused by dangling bonds. It is important to investigate defects in ion-implanted SiNWs since these carriers, intentionally introduced into SiNWs, are trapped by defect levels in the band gaps of SiNWs, ultimately making the dopant atoms electrically inactive. Hence, the Raman and ESR techniques are powerful methods for

* Address correspondence to fukata.naoki@nims.go.jp.

Received for review January 14, 2012 and accepted March 29, 2012.

Published online March 29, 2012
10.1021/nn300189z

© 2012 American Chemical Society

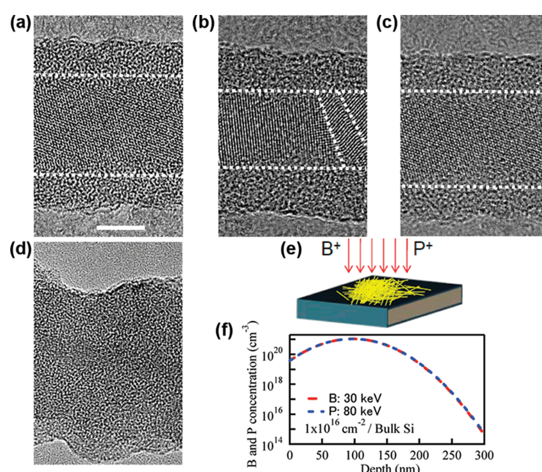

Figure 1. Typical TEM images of SiNWs (a) before ion implantation, and after ion implantation with a dose of (b) 1×10^{16} B^+/cm^2, (c) 5×10^{15} B^+/cm^2, and (d) 1×10^{16} P^+/cm^2. The activation annealing of dopant atoms was performed at 900 °C after implantation. SiNWs were synthesized using a $Si_{99}Ni_1$ target. The scale bar is 5 nm. (e) Illustration of ion implantation for SiNWs. (f) Depth profiles of B and P as estimated by TRIM.

investigating the crystallinity of the Si core, the states of dopant atoms, and defects in SiNWs.

In this paper, we report on the doping of B and P atoms into SiNWs by ion implantation, focusing on the use of micro-Raman scattering, ESR, and TEM measurements to elucidate the relationship between the recrystallization of the Si core of SiNWs and the reactivation of dopant atoms in SiNWs after thermal annealing. In particular, sufficiently high doses are necessary to form source and drain regions in NW MOSFETs, while the retardation of carrier mobility by the impurity scattering has to be considered for doping into the channel region. In order to suppress the impurity scattering, a core−shell NW using Si and Ge becomes a hopeful candidate. On the basis of these points, we focus on the effect of high influences in SiNWs.

RESULTS AND DISCUSSION

Figure 1a shows a typical high-resolution TEM image of SiNWs before ion implantation. It shows the Si lattice fringes inside the SiNW, revealing that the core comprises single-crystal Si sheathed with an amorphous SiO_x ($x \leq 2$) layer. Ion implantation was performed as shown in Figure 1e. After ion implantation at a dose of 1×10^{16} B^+/cm^2, the crystalline core became amorphous (Figure S1 in Supporting Information). This is due to the extensive disruption caused by ion implantation. To regain the crystallinity of the SiNWs, thermal annealing was performed at 900 °C. The results are shown in Figure 1b. The Si lattice fringes have clearly reappeared in the Si core region, but the structure is polycrystal, not single-crystal, indicating that nucleation occurs randomly in SiNWs, as described below. On the other hand, the core is single-crystal for SiNWs implanted with a dose of 5×10^{15} B^+/cm^2 and annealed at 900 °C, as shown in Figure 1c. Figure 1d shows a TEM image of P-implanted SiNWs after activation annealing at 900 °C. The dose is 1×10^{16} P^+/cm^2. Unlike with B implantation, the Si lattice fringes were not clearly visible, and the surface roughness was significantly higher. In the case of B implantation, the core changed to polycrystal at doses exceeding 1×10^{16} cm^{-2}, while for P implantation, polycrystal structures occur at doses above 1×10^{14} cm^{-2}. These are due to the greater damage caused by P implantation since the mass of P is greater than that of B. In this study, SiNWs were deposited on the SiO_2 substrates. Figure 1f shows the B and P depth profiles for bulk Si, simulated by TRIM. Similarly to the case for bulk Si, the concentration of impurity atoms implanted into SiNWs changes depending on the distance from the substrate. Therefore, we showed the TEM images of the most damaged SiNWs for each implantation dose. We also show results of Raman and ESR measurements for implanted SiNWs below. Considering the peak and signal intensities, the results are mainly reflected by SiNWs with high doping concentrations.

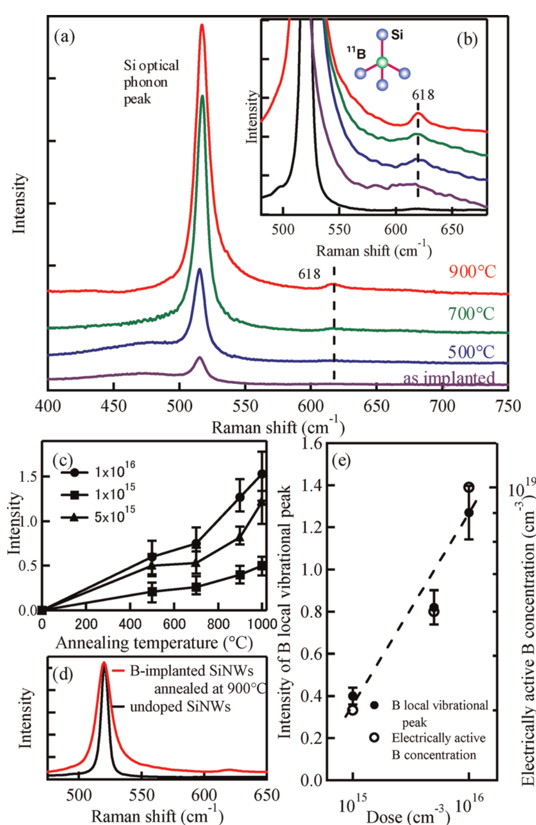

Figure 2. (a) Si optical phonon peak and B local vibrational peak observed for SiNWs after B ion implantation and subsequent activation annealing. (b) Magnified image of (a). (c) Dependence of the intensity of the B local vibrational peak on the annealing temperature. (d) Change in Si optical phonon peak before and after implantation with a dose of 1×10^{16} B^+/cm^2. (e) Dependence of the intensity of the B local vibrational peak and the electrically active B concentration on the ion implantation dose.

Raman scattering measurements were performed to investigate the recrystallization of SiNWs and the

reactivation of B acceptor atoms in SiNWs by activation annealing. The results are summarized in Figure 2. After B ion implantation, the Si optical phonon peak significantly decreased, and a broad peak related to amorphous Si appeared at around 470 cm^{-1}. The intensity of the Si optical phonon peak increased gradually with increasing annealing temperature and almost completely recovered after annealing at 900 °C. In addition to the increase in the Si optical phonon peak, the B local vibrational peak was observed at about 618 cm^{-1} (Figure 2b), showing that the B atoms were doped in Si substitutional sites in the crystalline Si core of SiNWs during the recrystallization process. The intensity of the B local vibrational peak also increased with increasing annealing temperature depending on the B ion dose (Figure 2c). The Si optical phonon peak showed a broadening toward a higher wavenumber with increasing annealing temperature. The broadening is clearly shown in Figure 2d, which shows a comparison with the result for undoped SiNWs. This broadening is due to the Fano effect, showing the presence of a high concentration of holes, namely, the reactivation of B atoms. Hence, these results clearly demonstrate the success of B doping by ion implantation. Two important fitting parameters, q (the asymmetry parameter) and Γ (the line width parameter), which are obtained by fitting using the Fano equation, were estimated to be about 20.1 and 6.9, respectively, for B-implanted SiNWs after annealing at 900 °C. The electrically active B concentration can be deduced to be on the order of 10^{19} cm^{-3} using the fitting values. Figure 2e shows the correlation between the peak intensity of the B local vibrational peak and the electrically active B concentration in B-implanted SiNWs. The result shows a good correlation between them. We can get a rough picture of the electrically active B concentration from the peak intensity of the B local vibrational peak. The activation efficiencies for each B-implanted SiNWs are almost the same with a value of about 10%. The low activation ratio is due to the compensation by residual defects, especially in samples implanted with higher doses. B atoms also easily segregate into the surface oxide layer during the activation annealing after ion implantation.[23] Hence, some B atoms probably located at the grain boundaries in the polycrystal, on interface between the SiO_2 and Si core, and in the surface oxide layer, resulting in a loss of electrical activity on the part of B atoms.

The recrystallization process of P-implanted SiNWs was also investigated by Raman scattering measurements. Instead of the Si optical phonon peak, a broad amorphous Si peak was observed after P ion implantation with a dose of 1×10^{16} cm^{-2} (Figure 3a). This indicates that the damage by P ion implantation is much greater than that for B ion implantation. The Si optical phonon peak shifted to a lower wavenumber after P ion implantation and the following activation

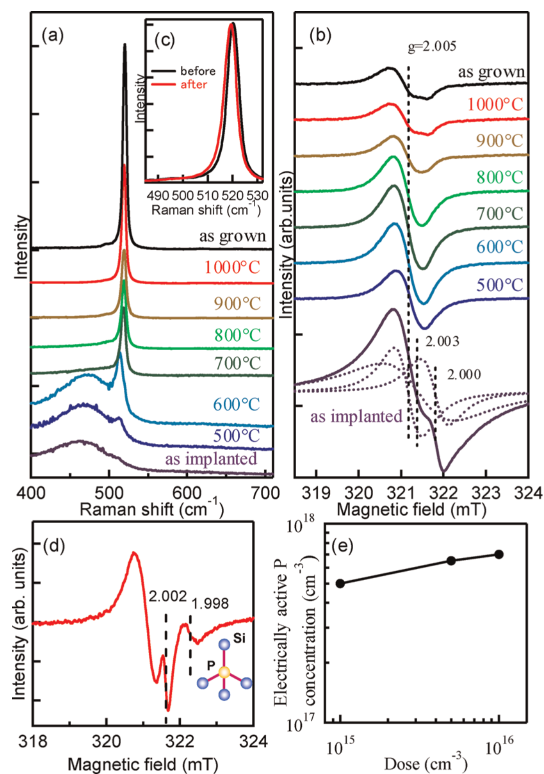

Figure 3. Annealing behaviors of (a) Si optical phonon peak and (b) ESR spectra observed for SiNWs implanted with 1×10^{16} P^+ cm^{-2}. (c) Change in the Si optical phonon peak before and after implantation with a dose of 1×10^{16} P^+/cm^2. ESR measurements were carried out at 4.2 K, and the microwave power was set at 1 mW. (d) ESR spectra observed at 20 K and 10 mW for P-ion-implanted SiNWs after annealing at 1000 °C. (e) Dependence of the electrically active P concentration on the ion implantation dose.

annealing (Figure 3b). As already shown in Figure 1d, the case of P implantation shows polycrystal structures in SiNWs, resulting in a downshift of the Si optical phonon peak due to the phonon confinement effect.[24] The Si optical phonon peak did not show the significant Fano broadening since the electrically active P concentration is too low to observe the Fano effect as described later. The Si optical phonon peak gradually increased, similarly to the case for B ion implantation. The annihilation of defects and electrical reactivation of P donors were investigated by ESR measurements at 4.2 K, as shown in Figure 3c. An ESR signal with a g value of 2.005 observed for as-grown SiNWs is due to the interfacial defects present at the interface between the surface and Si core of SiNWs before ion implantation.[20] After P ion implantation, the ESR signals comprise at least three signals. An ESR signal with almost the same g value of 2.005 was observed after P ion implantation. This ESR signal is assigned to defects in amorphous Si formed by P ion implantation,[25] while the ESR signals with g values of 2.003 and 2.000 are probably, respectively, assigned to defects called *EX* centers[26] and oxide-deficient defects called E' centers in the oxide layer[27] in SiNWs. The latter two defects were annihilated

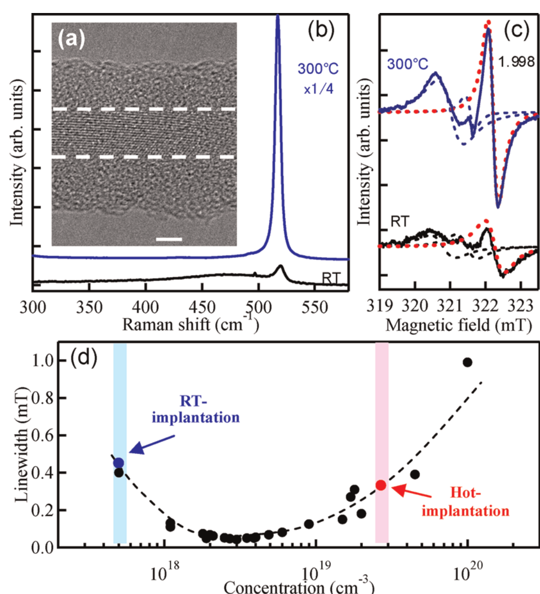

Figure 4. (a) TEM image of the SiNW after hot implantation at 300 °C. The scale bar is 2 nm. (b) Raman spectra and (c) ESR signals observed for SiNWs implanted with 1 × 10^{15} P^+ cm^{-2} at room temperature and 300 °C, respectively. Activation annealing was performed at 900 °C. (d) Dependence on P concentration of the ESR line width of conduction electrons.

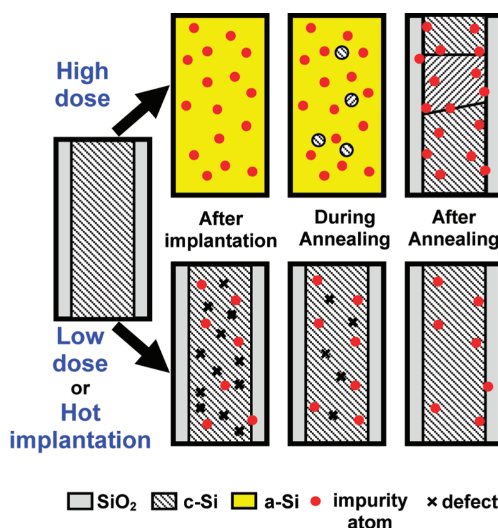

Figure 5. Schematic of the recrystallization process of ion-implanted SiNWs by thermal annealing.

by annealing at 500 °C. On the other hand, the annealing behavior of the former ESR signal is complicated, suggesting that the presence of two different defects may be the cause of this annealing behavior. The ESR signal decreased at 500 °C and then rose significantly. The first decrease is due to the annihilation of defects in amorphous Si induced by implantation, while the subsequent increase is due to the recrystallization of SiNWs, resulting in the reformation of the interface between the crystal Si core and the surface oxide layer and consequently the reformation of the interfacial defects at that location. The ESR signal again decreased on annealing at above 900 °C. This is due to the annihilation of excess interfacial defects during the formation process of the perfect interface by high-temperature annealing. After annealing at 1000 °C, the ESR signal of conduction electrons with a g value of 1.998 was observed (Figure 3d), showing that P atoms were doped in Si substitutional sites in the crystalline Si core of SiNWs and electrically activated at these sites, indicating the success of P doping by ion implantation. The electrically active P concentration can be roughly estimated as shown in Figure 3e. Contrary to the results of B-implanted SiNWs, the electrically active P concentration in SiNWs did not depend significantly on the ion implantation doses. The activation ratio is about 0.7, 1, and 5% for SiNWs implanted with 1 × 10^{16}, 5 × 10^{15}, and 1 × 10^{15} P^+ cm^{-3}, respectively, which are 2–3 orders of magnitude lower than the expected value from P ion implantation at room temperature. These are due to the greater damage caused by P implantation since the mass of P is greater than that of B. Recrystallization becomes more difficult with increasing ion dose since it results in the formation of polycrystals. Hence, the activation ratio decreases on increasing the ion dose for P-implanted SiNWs.

To suppress the formation of polycrystals in P-doped SiNWs, ion implantation was performed at 300 °C (hot implantation). Typical results for SiNWs implanted with a dose of 1 × 10^{15} P^+/cm^2 at RT and 300 °C are shown in Figure 4. The TEM image in Figure 4a shows that the Si core becomes single-crystal as a result of hot implantation. The intensity of the Si optical phonon peak significantly increased for the hot-implanted sample, as shown in Figure 4b. The ESR signal intensity of conduction electrons shown in Figure 4c also becomes significantly larger in hot implantation than in ordinary implantation at room temperature. This result clearly shows hot implantation to be a very useful method for realizing heavy ion implantation at high doses in SiNWs.

Figure 4d shows the ESR line width of P donor/conduction electrons as a function of P concentration. The ESR line width closely depends on the P concentration. The results of P-doped bulk Si[28,29] are shown in addition to our results for SiNWs. We plotted the ESR line widths obtained for P-doped SiNWs under the assumption that the relationship obtained for bulk Si is also true in SiNWs. We also plotted our data taking into account the ESR signal intensity, P doses, and crystallinity after activation annealing. The electrically active P concentrations in SiNWs implanted with 1 × 10^{16} and 1 × 10^{15} P^+/cm^2 are roughly estimated to be 7 × 10^{17} and 5 × 10^{17} cm^{-3}, respectively. The activation ratio is about 0.7–5%, which is 2–3 orders of magnitude lower than the expected value from P ion implantation at room temperature. On the other hand, the electrically active P concentration after hot implantation at a dose of 1 × 10^{15} P^+/cm^2 is estimated to be about 2 × 10^{19} cm^{-3}. This value is about 200-fold greater than the value

obtained for implantation at room temperature. The hot-implantation technique is thus proved to be extremely effective for impurity doping in SiNWs.

Finally, we discuss the recrystallization process of ion-implanted SiNWs by thermal annealing. The illustration is shown in Figure 5. The type of recrystallization closely depends on the implantation dose. High-dose implantation damages the crystal core and completely converts it to an amorphous state (Figure S1). Once the crystal Si core has been made amorphous, nucleation occurs randomly, resulting in the formation of a polycrystal Si core on thermal annealing since the initial crystal direction cannot be maintained. On the other hand, when the crystal Si core is only partially damaged, by low-dose implantation or hot implantation, the initial crystal direction is retained in the remaining crystal (Figure S1). Hence, nucleation readily occurs in the remaining crystal region as a result of thermal annealing, resulting in the formation of single crystals in SiNWs.

CONCLUSION

In conclusion, both B acceptors and P donors were implanted into SiNWs. The observation of B local vibrational peaks and the Fano broadening of the Si optical phonon peak showed the activation of B in the SiNWs: more specifically, the formation of p-type SiNWs. The ESR signal of conduction electrons with a *g* value of 1.998 also showed the activation of P in SiNWs, namely, the formation of n-type SiNWs. TEM images observed after activation annealing showed the recrystallization of the Si core of SiNWs, namely, polycrystal structures, not single crystals, on increasing the implantation dose. The hot-implantation technique was found to be useful for achieving single crystals and getting a higher reactivation rate of dopant atoms. We clearly showed not only the recrystallization process in SiNWs depending on the ion doses but also the detailed reactivation process and the electrical active concentration of dopant atoms (both B and P) with defect annihilation in SiNWs implanted with high fluences. In order to construct source and drain regions into SiNWs and realize next-generation MOSFET devices using them, it is indispensable to clarify the effect of high fluences. Hence these new findings will give us very useful information for the fabrication of next-generation MOSFET devices using SiNWs.

EXPERIMENTAL SECTION

SiNWs were synthesized at 1200 °C in flowing argon gas at 50 sccm by catalytic laser ablation[30] of a Si target with Ni as the metal catalyst ($Si_{99}Ni_1$). The targets were ablated using a frequency-doubled Nd:YAG laser (532 nm, 7 ns pulse width, 10 Hz, 150−180 mJ/pulse). The details of the laser ablation procedures are reported elsewhere.[24] SiNWs were directly deposited on a SiO_2 substrate to avoid the effects of the Si substrate. Growth was conducted by the so-called vapor−liquid−solid (VLS) mechanism.[31] SiNWs were implanted with 30 keV $^{11}B^+$ ions at doses ranging from 1×10^{13} to 1×10^{16} cm^{-2}. SiNWs were also implanted with 80 keV P^+ ions at the same doses. We determined the implantation energy by taking into account the thickness of deposited SiNWs; that is, we selected the ion energy that would introduce impurity atoms into all of the SiNWs deposited on the substrates. These implanted SiNW samples were annealed in an Ar gas atmosphere at 500−1000 °C for 30 min to electrically activate the dopant atoms.

Micro-Raman scattering measurements were performed at room temperature with a 100× objective and a 532 nm excitation light to investigate the states of the B atoms. The excitation powers were set at about 0.01−0.02 mW to avoid local heating effects by the excitation laser.[32] ESR measurements were carried out at 4.2 and 20 K using a X-band ESR spectrometer with 100 kHz magnetic field modulation to investigate the state of the P donors and defects in the SiNWs. SEM (scanning electron microscopy) (Hitachi S-4300, 30 kV) and TEM (transmission electron microscopy) (JEOL JEM4000EX, 400 kV) were used to observe the SiNWs and to investigate the details of their structures.

Conflict of Interest: The authors declare no competing financial interest.

Acknowledgment. This study was supported by the Japan Science and Technology Agency (JST). It was also partly supported by the Innovation Research Project on Nanoelectronics Materials and Structures, and the World Premier International Research Center Initiative (WPI Initiative), MEXT, Japan.

Supporting Information Available: Figure S1. This material is available free of charge *via* the Internet at http://pubs.acs.org.

REFERENCES AND NOTES

1. Cui, Y.; Duan, X.; Hu, J.; Lieber, C. M. Doping and Electrical Transport in Silicon Nanowires. *J. Phys. Chem. B* **2000**, *104*, 5213–5216.
2. Cui, Y.; Lieber, C. M. Functional Nanoscale Electronic Devices Assembled Using Silicon Nanowire Building Blocks. *Science* **2001**, *291*, 851–853.
3. Ma, D. D. D.; Lee, C. S.; Lee, S. T. Scanning Tunneling Microscopic Study of Boron-Doped Silicon Nanowires. *Appl. Phys. Lett.* **2001**, *79*, 2468–2470.
4. Lew, K. K.; Pan, L.; Bogart, T. E.; Dilts, S. M.; Dickey, E. C.; Redwing, J. M.; Wang, Y.; Cabassi, M.; Mayer, T. S.; Novak, S. W. Structural and Electrical Properties of Trimethylboron-Doped Silicon Nanowires. *Appl. Phys. Lett.* **2004**, *85*, 3101.
5. Zheng, G.; Lu, W.; Jin, S.; Lieber, C. M. Synthesis and Fabrication of High-Performance n-Type Silicon Nanowire Transistors. *Adv. Mater.* **2004**, *16*, 1890–1893.
6. Pan, L.; Lew, K. K.; Redwing, J. M.; Dickey, E. C. Effect of Diborane on the Microstructure of Boron-Doped Silicon Nanowires. *J. Cryst. Growth* **2005**, *277*, 428–436.
7. Wang, Y.; Lew, K. K.; Ho, T. T.; Pan, L.; Novak, S. W.; Dickey, E. C.; Redwing, J. M.; Mayer, T. S. Use of Phosphine as an n-Type Dopant Source for Vapor−Liquid−Solid Growth of Silicon Nanowires. *Nano Lett.* **2005**, *5*, 2139–2143.
8. Yang, C.; Zhong, Z.; Lieber, C. M. Encoding Electronic Properties by Synthesis of Axial Modulation-Doped Silicon Nanowires. *Science* **2005**, *310*, 1304–1307.
9. Tutuc, E.; Guha, S.; Chu, J. O. Morphology of Germanium Nanowires Grown in Presence of B_2H_6. *Appl. Phys. Lett.* **2006**, *88*, 043113.
10. Perea, D. E.; Hemesath, E. R.; Schwalbach, E. J.; Lensch-Falk, J. L.; Voorhees, P. W.; Lauhon, L. J. Direct Measurement of Dopant Distribution in an Individual Vapour−Liquid−Solid Nanowire. *Nat. Nanotechnol.* **2009**, *4*, 315–319.

11. Fukata, N.; Sato, K.; Mitome, M.; Bando, Y.; Sekiguchi, T.; Kirkham, M; Hong, J. I.; Wang, Z. L.; Snyder, R. L Doping and Raman Characterization of Boron and Phosphorus Atoms in Germanium Nanowires. *ACS Nano* **2010**, *4*, 3807–3816.
12. Chockla, A. M.; Korgel, B. A. Seeded Germanium Nanowire Synthesis in Solution. *J. Mater. Chem.* **2009**, *19*, 996–1001.
13. Colli, A.; Fasoli, A.; Ronning, C.; Pisana, S.; Piscanec, S.; Ferrari, A. C. Ion Beam Doping of Silicon Nanowires. *Nano Lett.* **2008**, *8*, 2188–2193.
14. Cohen, G. M.; Rooks, M. J.; Chu, J. O.; Laux, S. E.; Solomon, P. M.; Ott, J. A.; Miller, R. J.; Haensch, W. Nanowire Metal-Oxide-Semiconductor Field Effect Transistor with Doped Epitaxial Contacts for Source and Drain. *Appl. Phys. Lett.* **2007**, *90*, 233110.
15. Hayden, O.; Bjork, M. T.; Schmid, H.; Riel, H.; Drechsler, U.; Karg, S. F.; Lortscher, E.; Riess, W. Fully Depleted Nanowire Field-Effect Transistor in Inversion Mode. *Small* **2007**, *3*, 230–234.
16. Kanungo, P. D.; Kogler, R.; Nguyen-Duc, K.; Zakharov, N.; Werner, P.; Gosele, U. *Ex Situ* n and p Doping of Vertical Epitaxial Short Silicon Nanowires by Ion Implantation. *Nanotechnology* **2009**, *20*, 165706.
17. Kanungo, P. D.; Kogler, R.; Werner, P.; Gosele, U.; Skorupa, W. A Novel Method To Fabricate Silicon Nanowire p-n Junctions by a Combination of Ion Implantation and *In-Situ* Doping. *Nanoscale Res. Lett.* **2010**, *5*, 243–246.
18. Kanungo, P. D.; Kogler, R.; Zakharov, N.; Werner, P.; Scholz, R.; Skorupa, W. Characterization of Structural Changes Associated with Doping Silicon Nanowires by Ion Implantation. *Cryst. Growth. Des.* **2011**, *11*, 2690–2694.
19. Fukata, N.; Chen, J.; Sekiguchi, T.; Okada, N.; Murakami, K.; Tsurui, T.; Ito, S. Doping and Hydrogen Passivation of B in Silicon Nanowires Synthesized by Laser Ablation. *Appl. Phys. Lett.* **2006**, *89*, 203109.
20. Fukata, N.; Chen, J.; Sekiguchi, T.; Matsushita, S.; Oshima, T.; Uchida, N.; Murakami, K.; Tsurui, T.; Ito, S. Phosphorus Doping and Hydrogen Passivation of Donors and Defects in Silicon Nanowires Synthesized by Laser Ablation. *Appl. Phys. Lett.* **2007**, *90*, 153117.
21. Fukata, N.; Mitome, M.; Bando, Y.; Seoka, M.; Matsushita, S.; Murakami, K.; Chen, J.; Sekiguchi, T. Codoping of Boron and Phosphorus in Silicon Nanowires Synthesized by Laser Ablation. *Appl. Phys. Lett.* **2008**, *93*, 203106.
22. Fukata, N. Impurity Doping in Silicon Nanowires. *Adv. Mater.* **2009**, *21*, 2829–2832.
23. Fukata, N.; Ishida, S.; Yokono, S.; Takiguchi, R.; Chen, J.; Sekiguchi, T.; Murakami, K. Segregation Behaviors and Radial Distribution of Dopant Atoms in Silicon Nanowires. *Nano Lett.* **2011**, *11*, 651–656.
24. Fukata, N.; Oshima, T.; Murakami, K.; Kizuka, T.; Tsurui, T.; Ito, S. Phonon Confinement Effect of Silicon Nanowires Synthesized by Laser Ablation. *Appl. Phys. Lett.* **2005**, *86*, 213112.
25. Morehead, F. F.; Crowder, B. L.; Title, R. S. Formation of Amorphous Silicon by Ion Bombardment as a Function of Ion, Temperature, and Dose. *J. Appl. Phys.* **1972**, *43*, 1112–1118.
26. Baumer, A.; Stutzmann, M.; Brandt, M. S.; Au, F. C. K.; Lee, S. T. Paramagnetic Defects of Silicon Nanowires. *Appl. Phys. Lett.* **2004**, *85*, 943.
27. Griscom, D. L. E' Center in Glassy SiO_2: ^{17}O, ^{1}H, and "Very Weak" ^{29}Si Superhyperfine Structure. *Phys. Rev. B* **1980**, *22*, 4192–4202.
28. Maekawa, S.; Kinoshita, N. Electron Spin Resonance in Phosphorus Doped Silicon at Low Temperatures. *J. Phys. Soc. Jpn.* **1965**, *20*, 1447–1457.
29. Quirt, J. D.; Marko, J. R. Absolute Spin Susceptibilities and Other ESR Parameters of Heavily Doped n-Type Silicon. I. Metallic Samples. *Phys. Rev.* **1972**, *B5*, 1716–1728.
30. Morales, A. M.; Lieber, C. M. A Laser Ablation Method for the Synthesis of Crystalline Semiconductor Nanowires. *Science* **1998**, *279*, 208–211.
31. Wagner, R. S.; Ellis, W. C. Vapor−Liquid−Solid Mechanism of Single Crystal Growth. *Appl. Phys. Lett.* **1964**, *4*, 89–90.
32. Piscanec, S; Cantoro, M; Ferrari, A. C.; Zapien, J. A.; Lifshitz, Y.; Lee, S. T.; Hofmann, S.; Robertson, J. Raman Spectroscopy of Silicon Nanowires. *Phys. Rev. B* **2003**, *68*, 241312(R).